Combining linear-scaling quantum transport and machine-learning molecular dynamics to study thermal and electronic transports in complex materials

To cite this article: Zheyong Fan *et al* 2024 *J. Phys.: Condens. Matter* **36** 245901

OPEN ACCESS
IOP Publishing
Journal of Physics: Condensed Matter
J. Phys.: Condens. Matter **36** (2024) 245901 (8pp)
https://doi.org/10.1088/1361-648X/ad31c2

Combining linear-scaling quantum transport and machine-learning molecular dynamics to study thermal and electronic transports in complex materials

Zheyong Fan[1,*], Yang Xiao[1], Yanzhou Wang[2], Penghua Ying[3,*], Shunda Chen[4,*] and Haikuan Dong[1,*]

[1] College of Physical Science and Technology, Bohai University, Jinzhou 121013, People's Republic of China
[2] MSP Group, QTF Centre of Excellence, Department of Applied Physics, Aalto University, FI-00076 Aalto, Espoo, Finland
[3] Department of Physical Chemistry, School of Chemistry, Tel Aviv University, Tel Aviv 6997801, Israel
[4] Department of Civil and Environmental Engineering, George Washington University, Washington, DC 20052, United States of America

E-mail: brucenju@gmail.com, hityingph@163.com, phychensd@gmail.com and donghaikuan@163.com

Received 24 October 2023, revised 26 February 2024
Accepted for publication 8 March 2024
Published 21 March 2024

Abstract

We propose an efficient approach for simultaneous prediction of thermal and electronic transport properties in complex materials. Firstly, a highly efficient machine-learned neuroevolution potential (NEP) is trained using reference data from quantum-mechanical density-functional theory calculations. This trained potential is then applied in large-scale molecular dynamics simulations, enabling the generation of realistic structures and accurate characterization of thermal transport properties. In addition, molecular dynamics simulations of atoms and linear-scaling quantum transport calculations of electrons are coupled to account for the electron-phonon scattering and other disorders that affect the charge carriers governing the electronic transport properties. We demonstrate the usefulness of this unified approach by studying electronic transport in pristine graphene and thermoelectric transport properties of a graphene antidot lattice, with a general-purpose NEP developed for carbon systems based on an extensive dataset.

Keywords: machine-learned neuroevolution potential, molecular dynamics, thermal transport, linear-scaling quantum transport, electron-phonon scattering, electronic transport, thermoelectric transport

* Authors to whom any correspondence should be addressed.

1. Introduction

Thermal and electronic transports are two fundamental properties of a material. For simple solids, computational methods based on the electron and phonon Boltzmann transport equations [1] have been widely used to compute the transport properties mediated by the heat and charge carriers. There are a handful computational programs available for doing these calculations, such as SHENGBTE [2], PHONO3PY [3], KALDO [4], and GPUPBTE [5] for thermal transport and EPW [6], PERTURBO [7], and PHOEBE [8] for electronic transport. However, these methods can only efficiently deal with relatively simple systems and are generally not applicable to complex systems that cannot be properly represented by small periodic supercells.

To efficiently compute transport properties in complex systems one must resort to linear-scaling methods, i.e. methods with the computational cost that scales linearly with respect to the number of atoms in the periodic supercell. For thermal transport, molecular dynamics (MD) simulation is such a linear-scaling method at the atomistic level [9], provided that the interatomic potential used is a classical one and has a finite cutoff. Nowadays, machine-learned potentials (MLPs) [10] have been routinely applied in MD simulations of thermal transport. Particularly, the neuroevolution potential (NEP) [11–13] has been developed with a focus on thermal transport applications and has excellent computational efficiency.

For electronic transport, there are also linear-scaling quantum transport (LSQT) methods [14] based on semi-empirical tight-binding (TB) models. The electron-phonon coupling in LSQT calculations can be captured by the bond-length dependent hopping integrals in the electron TB Hamiltonian [15]. This has been explored using either specific phonon dynamics [16, 17] or MD simulations [18–20]. Static-disorder approximation of the electron-phonon coupling has also been used for organic crystals [21, 22], graphene [23] and a carbon nanotube [24]. Among these, the combined MD-LSQT approach is the most flexible one, but it has not been widely used. The major reason is that there has been no accurate interatomic potential to drive MD simulations for a general system. Another reason is that there is so far no publicly available implementation of this approach.

In this paper, we propose to combine machine-learning molecular dynamics (MLMD), namely, MD driven by a MLP, and LSQT with a bond-length-aware TB model, to study the thermal, electronic, and thermoelectric transport properties of complex materials that are beyond the reach of conventional methods. We call the combined method MLMD-LSQT. For the MLP, we choose to use the highly efficient NEP approach [11–13] as implemented in the *open-source* graphics processing units molecular dynamics (GPUMD) package [25]. By training against quantum-mechanical density functional theory (DFT) data, a NEP model can be constructed *on demand*, which can then be used to perform large-scale MD simulations to obtain realistic structures and thermal transport properties. For the LSQT part, we also implement it into the GPUMD package (version 3.9) to couple electron and ion motions. To show the usefulness of this unified approach, we construct a general-purpose NEP for carbon systems and study thermal, electronic, and thermoelectric transport properties of patterned graphene that has large-scale structural features.

2. The MLMD-LSQT approach

At the core of our method is the NEP approach [11–13] for MLP construction. It uses Chebyshev and Legendre polynomials to construct a local atom-environment descriptor of a given atom which is then mapped to the site energy U_i of this atom via a feed-forward neural network. The free parameters in the neural network as well as the descriptor are optimized through the minimization of a loss function using an evolutionary algorithm. The loss function is defined as a weighted sum of the root mean square errors (RMSEs) of energy, force, and virial between predictions and DFT target results in combination with regularization terms. This method as implemented in GPUMD [25] has been shown to be able to achieve simultaneously the accuracy of DFT calculations and the computational cost of empirical potentials, allowing for large-scale MD simulations up to 8.1 million atoms using a single 40-gigabyte graphics processing units (GPU) card [26].

The LSQT method can be used to calculate electrical conductivity in large systems, but the prerequisite is to construct an electron Hamiltonian incorporating electron-phonon coupling and other disorders [14]. By using a bond-length-aware TB model to configurations generated from MD simulations, electron-phonon coupling and other structural disorders can be effectively described. For dissipative electron transport, there are two equivalent ways to compute the electrical conductivity, one is based on the velocity-auto-correlation and the other is based on the mean-square displacement [14]. For the purpose of the present work, we found that the velocity-auto-correlation approach is more convenient because the time intervals used in the calculations are quite small, and the mean-square-displacement approach is only beneficial when the time intervals are large [27].

In the velocity-auto-correlation approach, the electrical conductivity at energy E and correlation time t can be calculated as an integral

$$\Sigma(E,t) = \frac{2e^2}{\Omega}\int_0^t \mathrm{Tr}\left[\delta\left(E-\hat{H}\right)\mathrm{Re}\left(\hat{V}\hat{V}(\tau)\right)\right]\mathrm{d}\tau, \qquad (1)$$

where e is the elementary charge, Ω is the system volume, $\hat{H}$ is the electron Hamiltonian operator, $\delta(E-\hat{H})$ is the energy resolution operator, $\hat{V}$ is the velocity operator, and $\hat{V}(\tau) = e^{i\hat{H}\tau}\hat{V}e^{-i\hat{H}\tau}$ is the time-evolved velocity operator. To facilitate the discussion, we denote the trace in the integral as $C(E,\tau)$. The coupled MLMD-LSQT algorithm can be represented as follows:

(i) Starting from an initial structure, run MLMD for a number of steps in the isothermal or isothermal-isobaric ensemble to achieve equilibrium.
(ii) Perform MLMD simulation for a number of steps:

(a) Evolve the atomic system from step $n-1$, $\{\boldsymbol{r}_i(n\Delta t - \Delta t)\}$, to step n, $\{\boldsymbol{r}_i(n\Delta t)\}$, by a time step of Δt according the NEP interatomic potential.
(b) Calculate the electron Hamiltonian and velocity operators at step n according to the atom positions $\{\boldsymbol{r}_i(n\Delta t)\}$.
(c) Calculate $C(E, n\Delta t)$ using the electron Hamiltonian at the current step. In this step, linear-scaling techniques [14], including sparse matrix-vector multiplication, random phase approximation of trace, Chebyshev expansion of quantum evolution operator, and kernel polynomial method [28] for energy resolution operator, are used.

After obtaining $C(E,\tau)$ at a number of discrete time points, it can be numerically integrated to calculate the electrical conductivity according to equation (1). This approach was implemented into the GPUMD package and was available starting from version 3.9. Besides, the electronic density of states (DOS) was also implemented according to the following expression:

$$\rho(E) = \frac{2}{\Omega}\mathrm{Tr}\left[\delta\left(E-\hat{H}\right)\right]. \tag{2}$$

3. Case study of a graphene antidot lattice

As a proof of concept, we apply the MLMD-LSQT approach to study the thermoelectric transport in a GAL [29], also known as graphene nanomesh [30], a graphene sheet with patterned holes. Thermoelectric effects in graphene nanostructures have been extensively studied, and GALs have been identified as one of the promising candidates for good thermoelectric materials [31]. However, previous works have only studied the ballistic electronic transport regime [32–34], without considering finite-temperature effects.

Figure 1 shows the atomistic structure of the system under investigation. The simulation domain cell of the GAL sample contains 187 200 atoms and has a dimension of about 88.5 nm × 76.7 nm in the xy-plane, which can be considered as a two-dimensional (2D) system when periodic boundary conditions are applied to the in-plane directions. The thickness of the system was taken as 0.335 nm in calculating the volume. The primitive cell for the GAL contains 156 atoms, a complexity that challenges conventional numerical methods based on the electron and phonon Boltzmann transport equations. However, this kind of complex structure are well-suited for the MLMD-LSQT approach. To construct the Hamiltonian and velocity operators, we employed a p_z-orbital TB model with a bond-length dependent hopping parameter

$$H_{ij} = t_0\left(\frac{r_0}{r_{ij}}\right)^2, \tag{3}$$

where $t_0 = -2.7$ eV, $r_0 = 1.42$ Å, and r_{ij} is the distance between the atom pair i and j. The model with a fixed hopping parameter t_0 has been used in previous works [35, 36] that did not account for electron-phonon coupling. The real-space Hamiltonian and velocity (assuming to be in the x direction) operators can be written as

$$\hat{H} = \sum_{i,j} H_{ij}|i\rangle\langle j|; \tag{4}$$

$$\hat{V} = \frac{i}{\hbar}\sum_{i,j}(x_j - x_i)H_{ij}|i\rangle\langle j|, \tag{5}$$

where x_i is the x-position of atom i.

3.1. Training a general-purpose NEP for carbon systems

Although for the scope of the current work, it suffices to train a specialized NEP model for GAL, it is our broader objective to train a general-purpose carbon potential based on the extensive dataset as used for constructing a Gaussian approximation potential [37]. Using this dataset and the hyperparameters given in appendix A, we trained a general-purpose NEP model for carbon systems. The training results are shown in figure 2. After a few hundred thousand training steps, the RMSEs of energy, force, and virial all converge (figure 2(a)), and their converged values are 45 meV/atom, 599 meV/Å, and 105 meV/atom, respectively. The predicted data are compared to the DFT reference ones in figures 2(b)–(d). The seemingly large RMSE values are typical for general-purpose carbon systems, as similar ones were reported in or can be extracted from previous works [13, 37–40].

3.2. Thermal transport

For a complete study of thermoelectric transport, the lattice (phonon) thermal conductivity κ_{ph} must be evaluated. To this end, we calculated κ_{ph} for the GAL model with 187 200 atoms using the HNEMD method [41]. In this method, an external driving force

$$\boldsymbol{F}_i^{\mathrm{ext}} = \boldsymbol{F}_{\mathrm{e}} \cdot \sum_{j\neq i}\left(\frac{\partial U_j}{\partial \boldsymbol{r}_{ji}} \otimes \boldsymbol{r}_{ij}\right) \tag{6}$$

is exerted on each atom i, driving the system out of equilibrium. Here, $\boldsymbol{F}_{\mathrm{e}}$ is the driving force parameter with the dimension of inverse length and $\boldsymbol{r}_{ij} \equiv \boldsymbol{r}_j - \boldsymbol{r}_i$, $\boldsymbol{r}_i$ being the position of atom i. After a steady state is achieved, the lattice thermal conductivity tensor $\kappa_{\mathrm{ph}}^{\alpha\beta}$ can be computed from the relation

$$\frac{\langle J^\alpha\rangle}{T\Omega} = \sum_\beta \kappa_{\mathrm{ph}}^{\alpha\beta} F_{\mathrm{e}}^\beta, \tag{7}$$

where T is the system temperature, Ω is the system volume, and $\langle J^\alpha\rangle$ is the ensemble average of the heat current [42]

$$\boldsymbol{J} = \sum_i \boldsymbol{v}_i \cdot \sum_{j\neq i}\left(\frac{\partial U_j}{\partial \boldsymbol{r}_{ji}} \otimes \boldsymbol{r}_{ij}\right). \tag{8}$$

In this case study, we only consider the condition of 300 K and zero in-plane pressure. The input script for GPUMD is

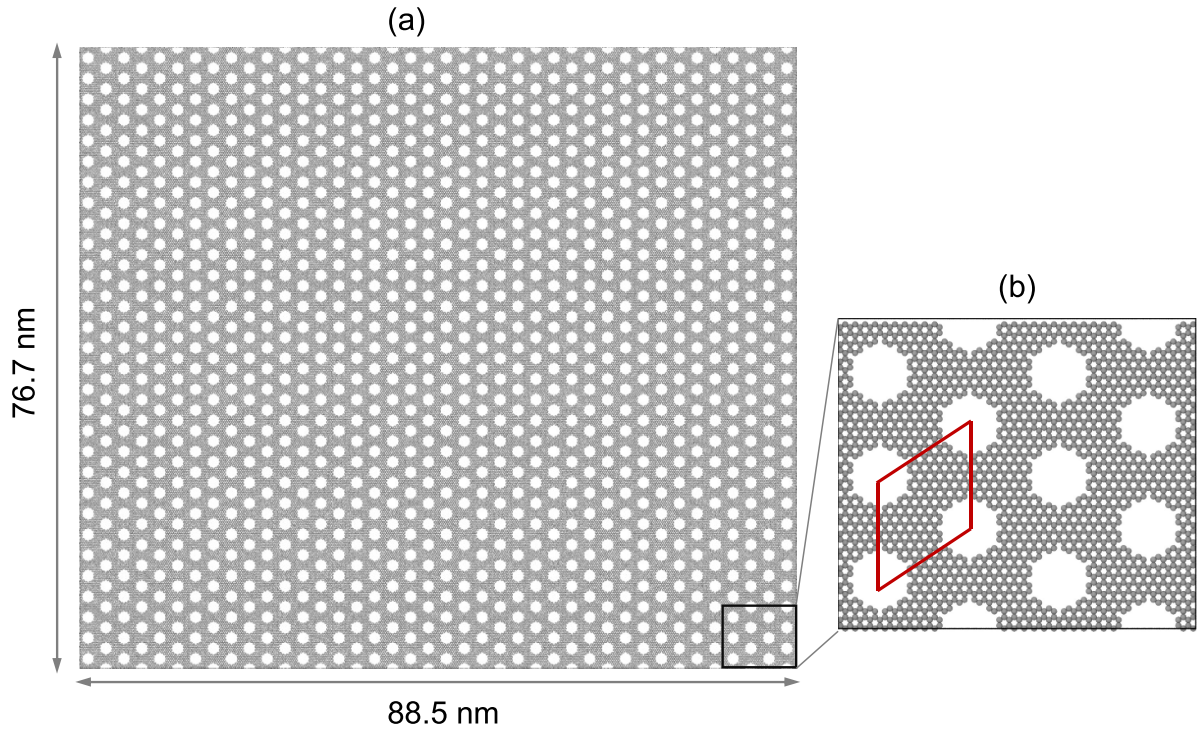

Figure 1. (a) Atomistic structure of an example graphene antidot lattice (GAL) system studied in this work. (b) Illustration of the primitive cell containing 156 atoms, enclosed by the parallelogram.

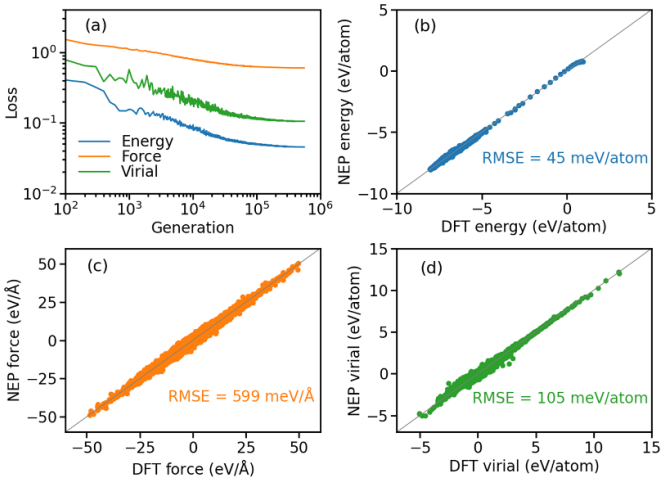

Figure 2. (a) Evolution of the energy, force, and virial loss values as a function of the number of training generations for a general-purpose NEP for carbon systems based on an extensive dataset [37]. (b)–(d) Comparison between NEP predictions and DFT reference values for energy, force, and virial. The RMSE values are indicated in each panel.

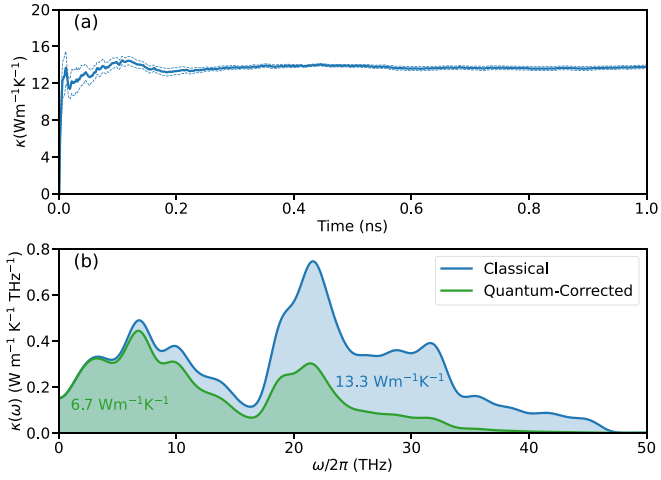

Figure 3. (a) Phonon thermal conductivity $\kappa_{\rm ph}$ as a function of the homogeneous non-equilibrium molecular dynamics (HNEMD) production time for GAL at 300 K. (b) The classical and quantum-corrected spectral thermal conductivity as a function of the phonon frequency $\omega/2\pi$.

given in appendix B. The time convergence of $\kappa_{\rm ph}$ is shown in figure 3(a). We have performed 4 independent simulations in both the x and the y directions and averaged the results over the two directions as the system is essentially isotropic.

For the GAL in our case study, the simulation temperature (300 K) is much lower than the Debye temperature (on the order of 2000 K), and the classical MD simulation thus significantly overestimates the modal heat capacity, which in turn leads to an overestimation of the thermal conductivity. Fortunately, there exists a feasible correction for the missing quantum statistics, as has been successfully applied to amorphous [43, 44] and fluid [45] systems described by NEP models. In this quantum correction method, the spectral thermal conductivity $\kappa(\omega)$ as calculated from the HNEMD method [41] is multiplied by a quantum-to-classical factor

$p(x) = x^2 e^x / (e^x - 1)^2$, where $x = \hbar\omega / k_B T$, ω is the phonon frequency, $\hbar$ is the reduced Planck constant, and k_B is the Boltzmann constant. The spectral decomposition of κ_{ph} corresponding to the classical results is depicted in figure 3(b), where the quantum-corrected results are also shown. The classical value of κ_{ph} is 13.3 $Wm^{-1}K^{-1}$, which becomes 6.7 $Wm^{-1}K^{-1}$ after quantum correction. The quantum corrected value will be used later.

3.3. Electronic and thermoelectric transports

We now move to study the electronic transport properties. Appendix C presents the input script and more calculation details. As a sanity check, we provide results for pristine graphene using the same TB model in appendix D.

The time-dependent electrical conductivity $\Sigma(E,t)$ converges in the diffusive transport regime, and one can obtain the so-called semi-classical electrical conductivity $\Sigma(E)$ by averaging $\Sigma(E,t)$ over a proper range of correlation time,

$$\Sigma(E) = \frac{1}{t_2 - t_1} \int_{t_1}^{t_2} \Sigma(E,t)\, \mathrm{d}t. \tag{9}$$

According to figure 4(a), it is a good choice to set $t_1 = 80$ fs and $t_2 = 100$ fs. The semi-classical electrical conductivity $\Sigma(E)$ can be regarded as the transport distribution function (TDF) [46–51] for thermoelectric transport. The calculated TDF as well as DOS are presented in figure 4(b). The anti-dots induce a considerable band gap of about 0.8 eV. This band gap is then also the transport gap.

From the TDF, we then calculated the transport coefficients at 300 K for a range of chemical potential μ. We first define the *functionals* ($n = 0, 1, 2$) of the TDF:

$$X_n(\mu,T) = \int \left[-\frac{\partial f(E,\mu,T)}{\partial E} \right] E^n \Sigma(E)\, \mathrm{d}E, \tag{10}$$

where

$$f(E,\mu,T) = \frac{1}{\exp\left(\frac{E-\mu}{k_B T}\right) + 1} \tag{11}$$

is the Fermi–Dirac distribution. The electrical conductivity $\sigma(\mu,T)$, Seebeck coefficient $S(\mu,T)$, and electronic thermal conductivity $\kappa_{el}(\mu,T)$ can be expressed in terms of these functionals as

$$\sigma(\mu,T) = X_0(\mu,T); \tag{12}$$

$$S(\mu,T) = -\frac{1}{eT}\left[\frac{X_1(\mu,T)}{X_0(\mu,T)} - \mu\right]; \tag{13}$$

$$\kappa_{el}(\mu,T) = \frac{1}{e^2 T}\left[X_2(\mu,T) - \frac{X_1^2(\mu,T)}{X_0(\mu,T)}\right]. \tag{14}$$

The calculated results are presented in figures 4(c)–(e). The finite-temperature electrical conductivity $\sigma(\mu,T)$ resembles the TDF, but with smearing resulting from the Fermi–Dirac distribution. The Seebeck coefficient has a negative peak for electrons and a positive peak for holes. The electronic thermal conductivity resembles the electrical conductivity in shape which is in line with the Wiedemann-Franz law.

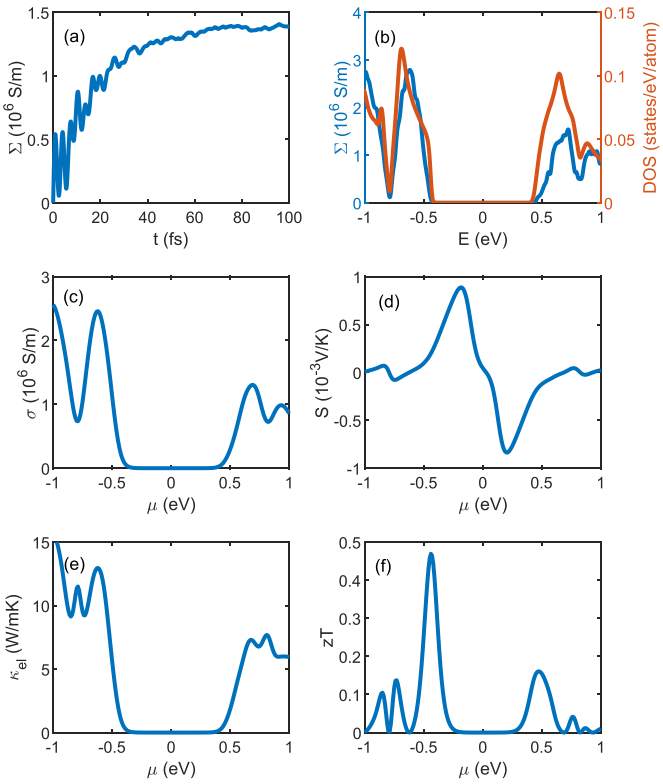

Figure 4. (a) Electrical conductivity $\Sigma(E,t)$ as computed by using equation (1) at $E = 0.65$ eV. (b) Transport distribution function (TDF) $\Sigma(E)$ and electronic density of states (DOS). (c)–(f) Electrical conductivity $\sigma(\mu,T)$, Seebeck coefficient $S(\mu,T)$, electronic thermal conductivity $\kappa_{el}(\mu,T)$, and figure of merit $zT(\mu,T)$ for a range of chemical potential μ at $T = 300$ K.

Based on these transport coefficients and the (quantum-corrected) phonon thermal conductivity κ_{ph}, one can define the dimensionless figure of merit as

$$zT(\mu,T) = \frac{S^2(\mu,T)\,\sigma(\mu,T)}{\kappa_{ph} + \kappa_{el}(\mu,T)} T. \tag{15}$$

Due to the competition between the various transport coefficients, zT develops peaks for both electron and hole transport, at $\mu = 0.47$ eV and -0.44 eV, respectively. The transport is asymmetric between electron and hole, showing a maximum $zT = 0.47$ for hole and a maximum $zT = 0.16$ for electron.

Experimentally, thermoelectric transport properties have been measured for single- and bi-layer graphene nanomeshes with the neck width down to 8 nm [52]. This neck width between the nearest antidot pairs is a few times larger than that we studied and the measured thermal conductivity values (of the order of 100 $Wm^{-1}K^{-1}$) are significantly larger than our prediction. On the other hand, there are geometrical disorders in the experimental samples, namely, variations in the positions and sizes of the antidots, which, according to previous calculations [35, 36], can lead to suppressed electrical

conductivity. Therefore, the relatively high zT values we predicted remain a challenge for experimental realization.

4. Summary and conclusions

In summary, we have introduced a numerical approach for simultaneous prediction of thermal and electronic transport properties in complex materials. This approach, based on MLMD and LSQT, offers an excellent efficiency with a computational cost that scales linearly with the system size. For a given material, a highly efficient NEP is first constructed *on demand*. This MLP can be used to perform large-scale MD to obtain realistic structures and accurate thermal transport properties. By combining the time-evolution of electrons and atoms during the MD simulation, electron-phonon scattering and other disorders for the charge carriers can be naturally captured and the various electronic transport properties can be obtained.

As an illustrative example, we have investigated the thermoelectric transport properties of a type of graphene antidot lattices (GALs) using our herein developed general-purpose NEP for carbon systems, predicting its relatively high thermoelectric efficiency at room temperature. We recognize the necessity of future work to conduct a more comprehensive study of the thermoelectric transport in GALs using our proposed approach. Subsequent research endeavors may consider integrating machine-learning techniques to explore the vast design space, similar to the methods employed in thermal transport studies in these systems [53, 54].

The accuracy of electronic transport calculations depends on both the machine-learned potential driving the MD and the environment-dependent TB model for electrons, which captures the electronic structures and electron-phonon coupling strength. While the NEP approach serves as a feasible candidate for accurate and efficient machine-learned potential, the development of accurate and efficient environment-dependent TB models using machine-learning techniques remains relatively unexplored. We believe it is possible to extend the NEP approach to the TB model and integrate it into our unified approach. This possibility is left for future work.

Furthermore, it is worth noting that the classical statistics in MD simulation might also lead to overestimated electron-phonon coupling due to overpopulated high-frequency phonons. A quantum correction scheme similar to that used in phonon thermal transport may be feasible. However, this topic is also left for future investigation.

Data availability statement

The data that support the findings of this study are openly available at the following URL/DOI: https://gitlab.com/brucefan1983/nep-data. Complete input and output files for the general-purpose carbon NEP model are freely available at https://gitlab.com/brucefan1983/nep-data. The source code and documentation for GPUMD are available at https://github.com/brucefan1983/GPUMD and https://gpumd.org, respectively.

Acknowledgments

Z Fan and H Dong were supported by the National Natural Science Foundation of China (NSFC) (No. 11974059) and the Research Fund of Bohai University (No. 0522xn076). P Ying was supported by the Israel Academy of Sciences and Humanities & Council for Higher Education Excellence Fellowship Program for International Postdoctoral Researchers.

Conflict of interest

The authors declare that they have no conflict of interest.

Appendix A. Inputs for training the NEP model

NEP models can be trained using the `nep` executable in the GPUMD package. The relevant hyperparameters are specified in the `nep.in` input file. The contents of the `nep.in` input file for training the general-purpose model of carbon systems are given below.

```
type       1 C
version    4
cutoff     7  4
n_max      12 8
basis_size 16 12
l_max      4 2 1
neuron     100
lambda_1   0.0
lambda_e   1.0
lambda_v   0.1
batch      8000
population 100
generation 2000000
```

Appendix B. Inputs for phonon thermal conductivity calculations

MD simulations with NEP models can be performed by using the `gpumd` executable in the GPUMD package. The controlling parameters are specified in the `run.in` input file. The contents of the `run.in` input file for calculating the thermal conductivity are given below.

```
# setup
potential  nep.txt
velocity  300

# equilibration
ensemble   npt_ber 300 300 100 0 0 0
           1000 1000 1000 1000
time_step  1
```

```
run           100000

# production
ensemble      nvt_nhc 300 300 100
compute_hnemd 1000 1e-4 0 0
compute_shc   2 250 0 1000 400.0
run           1000000
```

Appendix C. Inputs for electronic transport calculations

The contents of the `run.in` input file for calculating the electronic transport properties are given below. The time step in the production stage is chosen to be small enough (0.1 fs) to ensure accurate integration in equation (1). The keyword `compute_lsqt` invokes the LSQT calculations. This is a new keyword introduced in GPUMD-v3.9 during the course of the present study. Here are the meanings of the parameters for this keyword:

- The first parameter `x` means that the transport is along the x direction. We have calculated 10 times along the x directions and also 10 times along the y direction and averaged the results.
- The second parameter refers to the number of Chebyshev moments in the kernel-polynomial method [28] for both the DOS and conductivity calculations. A value of 3000 is large enough here.
- The next three parameters are respectively the number of energy points to be considered, the minimum energy and the maximum energy. Here we calculated the transport properties from -8.1 eV to 8.1 eV, with an interval of 1.62 meV.
- The last parameter is an energy threshold that needs to be larger than the energy range of the TB model. Here, a value of 8.2 eV is sufficient. This parameter can be determined by a trial-and-error approach.

```
#setup
potential    nep.txt
velocity     300

# equilibration
ensemble     npt_ber 300 300 100 0 0 0
             1000 1000 1000 1000
time_step    1
dump_exyz    100000
run          100000

# production
ensemble     nve
time_step    0.1
compute_lsqt x 3000 10001 -8.1 8.1 8.2
run          1000
```

Appendix D. Benchmark study of pristine graphene

To model electronic transport in pristine graphene, we adopted the same TB model as used for GAL. We constructed an almost square-shaped graphene sheet with 864 000 atoms.

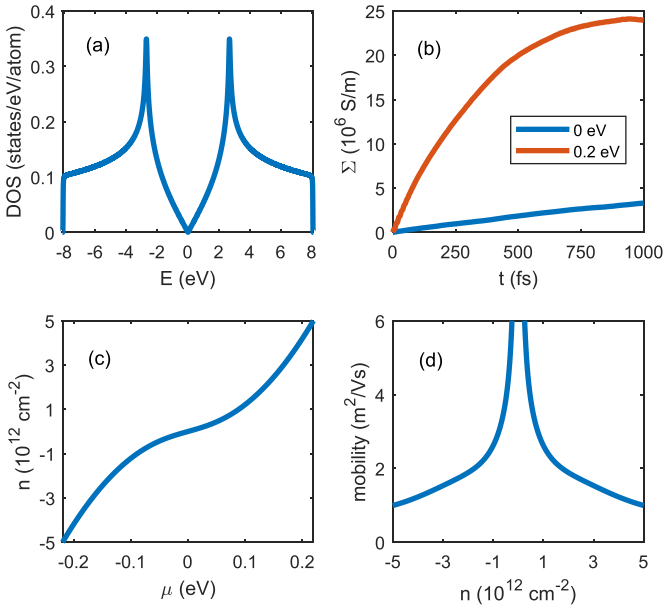

Figure D1. (a) Electronic density of states (DOS). (b) Electrical conductivity $\Sigma(E,t)$ as computed by using equation 1 at $E = 0$ eV and $E = 0.2$ eV. (c) Carrier concentration n as a function of chemical potential μ at $T = 300$ K. (d) Mobility as a function of carrier concentration n at $T = 300$ 'K. The predicted mobility values are in excellent agreement with the measured values reported by Novoselov *et al* for the very first graphene-based field effect transistor at room temperature [55].

The `run.in` input file used for GAL also applies to pristine graphene, but the time step in the production stage is changed to 1 fs due to the much larger relaxation times in pristine graphene.

Results for the temperature of $T = 300$ K are shown in figure D1. The DOS (figure D1(a)) resembles that for pristine graphene at zero temperature [27], even though we are considering 300 K. The time-dependent electrical conductivity $\Sigma(E,t)$ is well-converged up to $t = 1000$ fs for $E = 0.2$ eV, but not for the Dirac point $E = 0$ eV (figure D1(b)). Fortunately, for realistic carrier concentrations (of the order of 10^{12} cm^2), the relevant energies are away from the Dirac point, as shown in figure D1(c). The carrier concentration (positive values for electrons and negative for holes) is calculated as

$$n(\mu,T) = \int \rho(E) f(E,\mu,T)\,\mathrm{d}E. \tag{D1}$$

From the electrical conductivity $\sigma(\mu,T)$ and the carrier concentration, we can obtain the carrier mobility as

$$\text{mobility} = \frac{1}{e}\frac{\sigma(\mu,T)}{|n(\mu,T)|}. \tag{D2}$$

The results are shown in figure D1(d). The mobility is as high as about 10 000 cm^2 Vs^{-1} even at a high carrier concentration of $n = 5 \times 10^{12}$ cm^{-2}, and reaches about 26 000 cm^2 Vs^{-1} when n is reduced to 10^{12} cm^{-2}. These values are in excellent agreement with the measured values reported by Novoselov *et al* for the very first graphene-based field effect transistor at room temperature [55].

ORCID iDs

Zheyong Fan https://orcid.org/0000-0002-2253-8210
Penghua Ying https://orcid.org/0000-0002-5758-2369
Shunda Chen https://orcid.org/0000-0002-5506-7507
Haikuan Dong https://orcid.org/0000-0001-9870-0467

References

[1] Ziman J M 2001 *Electrons and Phonons: The Theory Of Transport Phenomena in Solids* (Oxford University Press)
[2] Li W, Carrete J, Katcho N A and Mingo N 2014 *Comput. Phys. Commun.* **185** 1747–58
[3] Togo A, Chaput L and Tanaka I 2015 *Phys. Rev.* B **91** 094306
[4] Barbalinardo G, Chen Z, Lundgren N W and Donadio D 2020 *J. Appl. Phys.* **128** 135104
[5] Zhang B, Fan Z, Zhao C Y and Gu X 2021 *J. Phys.: Condens. Matter* **33** 495901
[6] Poncé S, Margine E, Verdi C and Giustino F 2016 *Comput. Phys. Commun.* **209** 116–33
[7] Zhou J J, Park J, Lu I T, Maliyov I, Tong X and Bernardi M 2021 *Comput. Phys. Commun.* **264** 107970
[8] Cepellotti A, Coulter J, Johansson A, Fedorova N S and Kozinsky B 2022 *J. Phys. Mater.* **5** 035003
[9] Gu X, Fan Z and Bao H 2021 *J. Appl. Phys.* **130** 210902
[10] Behler J 2016 *J. Chem. Phys.* **145** 170901
[11] Fan Z, Zeng Z, Zhang C, Wang Y, Song K, Dong H, Chen Y and Ala-Nissila T 2021 *Phys. Rev.* B **104** 104309
[12] Fan Z 2022 *J. Phys.: Condens. Matter* **34** 125902
[13] Fan Z *et al* 2022 *J. Chem. Phys.* **157** 114801
[14] Fan Z, Garcia J H, Cummings A W, Barrios-Vargas J E, Panhans M, Harju A, Ortmann F and Roche S 2021 *Phys. Rep.* **903** 1–69
[15] Goringe C M, Bowler D R and Hernández E 1997 *Rep. Prog. Phys.* **60** 1447
[16] Roche S, Jiang J, Triozon F M C and Saito R 2005 *Phys. Rev. Lett.* **95** 076803
[17] Roche S, Jiang J, Triozon F M C and Saito R 2005 *Phys. Rev.* B **72** 113410
[18] Ishii H, Triozon F, Kobayashi N, Hirose K and Roche S 2009 *C. R. Physique* **10** 283–96
[19] Ishii H, Kobayashi N and Hirose K 2010 *Phys. Rev.* B **82** 085435
[20] Ishii H, Roche S, Kobayashi N and Hirose K 2010 *Phys. Rev. Lett.* **104** 116801
[21] Ortmann F and Roche S 2011 *Phys. Rev.* B **84** 180302
[22] Ciuchi S, Fratini S and Mayou D 2011 *Phys. Rev.* B **83** 081202
[23] Fan Z, Uppstu A and Harju A 2017 *2D Mater.* **4** 025004
[24] Fan Z, Vierimaa V and Harju A 2018 *Comput. Phys. Commun.* **230** 113–20
[25] Fan Z, Chen W, Vierimaa V and Harju A 2017 *Comput. Phys. Commun.* **218** 10–16
[26] Liu J, Byggmästar J, Fan Z, Qian P and Su Y 2023 *Phys. Rev.* B **108** 054312
[27] Fan Z, Uppstu A, Siro T and Harju A 2014 *Comput. Phys. Commun.* **185** 28–39
[28] Weiße A, Wellein G, Alvermann A and Fehske H 2006 *Rev. Mod. Phys.* **78** 275–306
[29] Pedersen T G, Flindt C, Pedersen J, Mortensen N A, Jauho A P and Pedersen K 2008 *Phys. Rev. Lett.* **100** 136804
[30] Bai J, Zhong X, Jiang S, Huang Y and Duan X 2010 *Nat. Nanotechnol.* **5** 190–4
[31] Dollfus P, Nguyen V H and Saint-Martin J 2015 *J. Phys.: Condens. Matter* **27** 133204
[32] Gunst T, Markussen T, Jauho A P and Brandbyge M 2011 *Phys. Rev.* B **84** 155449
[33] Karamitaheri H, Pourfath M, Faez R and Kosina H 2011 *J. Appl. Phys.* **110** 054506
[34] Yan Y, Liang Q F, Zhao H, Wu C Q and Li B 2012 *Phys. Lett.* A **376** 2425–9
[35] Pedersen J G, Cummings A W and Roche S 2014 *Phys. Rev.* B **89** 165401
[36] Fan Z, Uppstu A and Harju A 2015 *Phys. Rev.* B **91** 125434
[37] Rowe P, Deringer V L, Gasparotto P, Csányi G and Michaelides A 2020 *J. Chem. Phys.* **153** 034702
[38] Wang J, Shen H, Yang R, Xie K, Zhang C, Chen L, Ho K M, Wang C Z and Wang S 2022 *Carbon* **186** 1–8
[39] Wang Y, Fan Z, Qian P, Ala-Nissila T and Caro M A 2022 *Chem. Mater.* **34** 617–28
[40] Qamar M, Mrovec M, Lysogorskiy Y, Bochkarev A and Drautz R 2023 *J. Chem. Theory Comput.* **19** 5151–67
[41] Fan Z, Dong H, Harju A and Ala-Nissila T 2019 *Phys. Rev.* B **99** 064308
[42] Fan Z, Pereira L F C, Wang H Q, Zheng J C, Donadio D and Harju A 2015 *Phys. Rev.* B **92** 094301
[43] Wang Y, Fan Z, Qian P, Caro M A and Ala-Nissila T 2023 *Phys. Rev.* B **107** 054303
[44] Zhang H, Gu X, Fan Z and Bao H 2023 *Phys. Rev.* B **108** 045422
[45] Xu K, Hao Y, Liang T, Ying P, Xu J, Wu J and Fan Z 2023 *J. Chem. Phys.* **158** 204114
[46] Mahan G D and Sofo J O 1996 *Proc. Natl Acad. Sci.* **93** 7436–9
[47] Fan Z, Wang H Q and Zheng J C 2011 *J. Appl. Phys.* **109** 073713
[48] Zhou J, Yang R, Chen G and Dresselhaus M S 2011 *Phys. Rev. Lett.* **107** 226601
[49] Jeong C, Kim R and Lundstrom M S 2012 *J. Appl. Phys.* **111** 113707
[50] Maassen J 2021 *Phys. Rev.* B **104** 184301
[51] Ding S, Chen X, Xu Y and Duan W 2023 *npj Comput. Mater.* **9** 189
[52] Oh J *et al* 2017 *Nano Energy* **35** 26–35
[53] Wan J, Jiang J W and Park H S 2020 *Carbon* **157** 262–9
[54] Wei H, Bao H and Ruan X 2020 *Nano Energy* **71** 104619
[55] Novoselov K S, Geim A K, Morozov S V, Jiang D, Zhang Y, Dubonos S V, Grigorieva I V and Firsov A A 2004 *Science* **306** 666–9